High contrast 40Gbit/s optical modulation in silicon

D. J. Thomson,[1,*] F. Y. Gardes,[1] Y. Hu,[1] G. Mashanovich,[1] M. Fournier,[2] P. Grosse,[2] J-M. Fedeli[2] and G. T. Reed[1]

[1]*Advanced Technology Institute, University of Surrey, Guildford, Surrey, UK*
[2]*CEA,LETI, Minatec 17 rue des Martyrs 38054 Grenoble France*
[*]*d.thomson@surrey.ac.uk*

Abstract: Data interconnects are on the verge of a revolution. Electrical links are increasingly being pushed to their limits with the ever increasing demand for bandwidth. Data transmission in the optical domain is a leading candidate to satisfy this need. The optical modulator is key to most applications and increasing the data rate at which it operates is important for reducing power consumption, increasing channel bandwidth limitations and improving the efficiency of infrastructure usage. In this work silicon based devices of lengths 3.5mm and 1mm operating at 40Gbit/s are demonstrated with extinction ratios of up to 10dB and 3.5dB respectively. The efficiency and optical loss of the phase shifter is 2.7V.cm and 4dB/mm (or 4.5dB/mm including waveguide loss) respectively.

OCIS codes: (130.4110) Modulators; (060.4080) Modulation.

References and links

1. G. T. Reed, G. Mashanovich, F. Y. Gardes, and D. J. Thomson, "Silicon optical modulators," Nat. Photonics **4**(8), 518–526 (2010).
2. F. Y. Gardes, A. Brimont, P. Sanchis, G. Rasigade, D. Marris-Morini, L. O'Faolain, F. Dong, J.-M. Fedeli, P. Dumon, L. Vivien, T. F. Krauss, G. T. Reed, and J. Martí, "High-speed modulation of a compact silicon ring resonator based on a reverse-biased pn diode," Opt. Express **17**(24), 21986–21991 (2009).
3. P. Dong, S. Liao, D. Feng, H. Liang, D. Zheng, R. Shafiiha, C.-C. Kung, W. Qian, G. Li, X. Zheng, A. V. Krishnamoorthy, and M. Asghari, "Low Vpp, ultralow-energy, compact, high-speed silicon electro-optic modulator," Opt. Express **17**(25), 22484–22490 (2009).
4. J.-B. You, M. Park, J.-W. Park, and G. Kim, "12.5 Gbps optical modulation of silicon racetrack resonator based on carrier-depletion in asymmetric p-n diode," Opt. Express **16**(22), 18340–18344 (2008).
5. D. Marris-Morini, X. Le Roux, L. Vivien, E. Cassan, D. Pascal, M. Halbwax, S. Maine, S. Laval, J. M. Fédéli, and J. F. Damlencourt, "Optical modulation by carrier depletion in a silicon PIN diode," Opt. Express **14**(22), 10838–10843 (2006).
6. C. Gunn, "CMOS photonics for high-speed interconnects," Micro. IEEE **26**(2), 58–66 (2006).
7. J. W. Park, J.-B. You, I. G. Kim, and G. Kim, "High-modulation efficiency silicon Mach-Zehnder optical modulator based on carrier depletion in a PN Diode," Opt. Express **17**(18), 15520–15524 (2009).
8. A Narasimha, S. Abdaila, C. Bradbury, A. Clark, J. Clymore, J. Coyne, A. Dahl, S. Gloeckner, A. Gruenberg, D. Guckenberger, S. Gutierrez, M. Harrison, D. Kucharski, K. Leap, R. LeBlanc, V. Liang, M. Mack, D. Martinez, G. Masini, A. Mekis, R. Menigoz, C. Ogden, M. Peterson, T. Pinguet, J. Redman, J. Rodriguez, S. Sahni, M. Sharp, T. J. Sleboda, D. Song, V. Wang, B. Welch, J. Witzens, W. Xu, K. Vokoyama and P. D. DobbeIaere "An ultra low power CMOS photonics technology platform for H/S optoelectronic transceivers at less than $1 per Gbps," *in Proc. OFC 2010*, San Diego, USA (2010).
9. L. Tsung-Yang, A. Kah-Wee, F. Qing, S. Jun-Feng, X. Yong-Zhong, Y. Ming-Bin, L. Guo-Qiang, and K. Dim-Lee, "Silicon modulators and germanium photodetectors on SOI: Monolithic integration, compatibility, and performance optimization," IEEE J. Sel. Top. Quantum Electron. **16**(1), 307–315 (2010).
10. D. M. Gill, M. Rasras, K.-Y. Tu, Y.-K. Chen, A. E. White, S. S. Patel, D. Carothers, A. Pomerene, R. Kamocsai, C. Hill, and J. Beattie, "Internal bandwidth equalization in a CMOS compatible si ring modulator," IEEE Photon. Technol. Lett. **21**(4), 200–202 (2009).
11. S. J. Spector, M. W. Geis, M. E. Grein, R. T. Schulein, J. U. Yoon, D. M. Lennon, F. Gan, G.-R. Zhou, F. X. Kaertner, and T. M. Lyszczarz, "High-speed silicon electro-optical modulator that can be operated in carrier depletion or carrier injection mode," 2008 Conference on Lasers and Electro-Optics (CLEO), (2008).

#144357 - $15.00 USD Received 23 Mar 2011; revised 22 May 2011; accepted 23 May 2011; published 31 May 2011

12. N.-N. Feng, S. Liao, D. Feng, P. Dong, D. Zheng, H. Liang, R. Shafiiha, G. Li, J. E. Cunningham, A. V. Krishnamoorthy, and M. Asghari, "High speed carrier-depletion modulators with 1.4V-cm V(π)L integrated on 0.25microm silicon-on-insulator waveguides," Opt. Express **18**(8), 7994–7999 (2010).
13. M. R. Watts, W. A. Zortman, D. C. Trotter, R. W. Young, and A. L. Lentine, "Low-Voltage, Compact, Depletion-Mode, Silicon Mach–Zehnder Modulator," IEEE J. Sel. Top. Quantum Electron. **16**(1), 159–164 (2010).
14. D. J. Thomson, F. Y. Gardes, G. T. Reed, F. Milesi, and J.-M. Fedeli, "High speed silicon optical modulator with self aligned fabrication process," Opt. Express **18**(18), 19064–19069 (2010).
15. L. Liao, A. Liu, D. Rubin, J. Basak, Y. Chetrit, H. Nguyen, R. Cohen, N. Izhaky, and M. Paniccia, "40 Gbit/s silicon optical modulator for high speed applications," Electron. Lett. **43**(22), 1196–1197 (2007).
16. D. J. Thomson, Y. Hu, G. T. Reed, and J.-M. Fedeli, "Low loss MMI couplers for high performance MZI modulators," Photon. Technol. Lett. **22**(20), 1485–1487 (2010).
17. G. T. Reed and A. P. Knights, "Silicon photonics- An introduction," Wiley, ISBN 0–470–87034–6 (2004).

1. Introduction

Photonic components formed in silicon offer an exciting future for a number of different applications. The prospect of integrating both CMOS and photonics on the same substrate can offer cost reductions, performance enhancements and added functionality. This has fuelled an increasing interest in the field of silicon photonics and has spurred a period of rapid development. The optical modulator, which writes data onto an optical carrier, is one of several components in silicon-on-insulator which have experienced dramatic performance enhancements over the previous decade. The most successful demonstrations of optical modulation in silicon have come from devices based upon the plasma dispersion effect which relates changes in the electron and hole concentration to changes in refractive index. Devices of this type which employ carrier depletion to electrically manipulate the free carrier densities have emerged in recent years as the leader in terms of performance, fabrication simplicity and CMOS compatibility [1]. These devices generally use a pn diode structure which is positioned with the junction in or around an optical rib waveguide such that the depletion region, whose width changes with applied reverse bias, interacts with the light propagating along the waveguide. A change in the phase of the light exiting the waveguide then occurs with changing depletion width due to the resultant change in effective refractive index. In recent years an abundance of devices following this approach have been reported demonstrating a performance at or around 10Gbit/s [2–14].

Whilst data transmission at 10Gbit/s is sufficient for many current applications, the primary advantages of using 40Gbit/s over lower data rates are threefold. Firstly the usable bandwidth of the channel is increased, making better use of in situ infrastructure as well as infrastructure currently being installed. Secondly the power consumption for each bit of data is reduced, lessening the burden on heat sinking and providing a more environmentally friendly solution. Thirdly, if multiple channels are used to increase the aggregate data rate, a higher data rate per channel reduces the number of channels required. A 40Gbit/s modulator has previously been demonstrated in silicon, although only 1dB of modulation depth was achieved making it impractical for use in most applications [15]. In this work, data is presented from a carrier depletion modulator operating at 40Gbit/s with a modulation depth of up to 10dB making the device viable for a number of applications.

2. Device design and fabrication

The modulator comprises a phase shifter (or phase modulator), fabricated in a Mach-Zehnder interferometer. A diagram of the phase shifter cross-section is shown in Fig. 1. The device is based upon carrier depletion in a reverse biased pn junction and whose fabrication was performed using a CMOS compatible process steps. The rib section of the waveguide and slab to one side are formed of p type silicon. The slab region to the other side of the waveguide rib is formed of n-type silicon. The p and n type regions contact p+ and n+ regions respectively to provide ohmic contacts to coplanar waveguide electrodes which are used to drive the device.

#144357 - $15.00 USD Received 23 Mar 2011; revised 22 May 2011; accepted 23 May 2011; published 31 May 2011

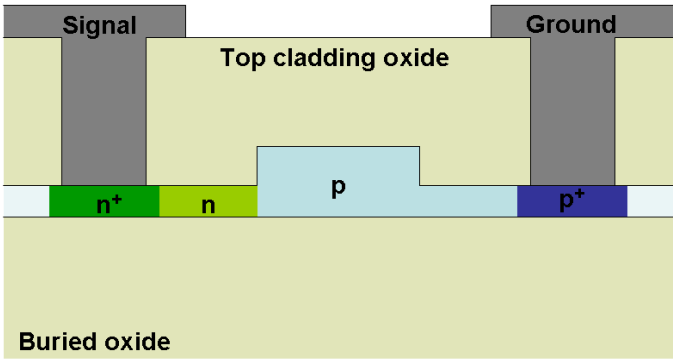

Fig. 1. Diagram showing the phase shifter cross-section

An advantage of this device design is the simplicity of the fabrication process used to form the device. In previously reported devices the pn junction is positioned within the waveguide rib region necessitating critical alignment of the doping steps [2–4, 6–12]. Alignment errors are typical of any fabrication process and can result in device performance variations or even failure. In the electronics industry self-aligned processes have been used for many years to mitigate against possible performance variations and yield reductions. The positioning of the pn junction at the edge of the rib in this device permits the use of a self-aligned process in its formation as depicted in Fig. 2.

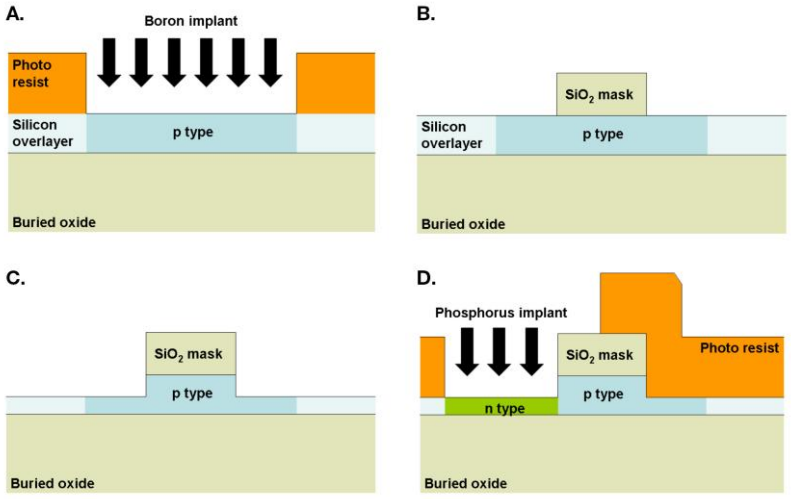

Fig. 2. Diagram showing the self-aligned formation of the pn junction. (a) – The active region is implanted with boron making the region p type. (b) – A silicon dioxide layer deposited onto the surface is patterned with the waveguide design. (c) – The waveguide is etched into the silicon overlayer using the silicon dioxide layer as a mask. (d) – A photoresist window is opened on one side of the waveguide through which phosphorus ions are implanted to form an n type region at the side of the waveguide.

The active region of the device is first implanted with boron ions, making it p type. A silicon dioxide layer is then deposited onto the surface and patterned with the waveguide design. This silicon dioxide layer is used firstly as the hard-mask through which to etch the waveguides. It is then used in conjunction with a photoresist window as a mask for the phosphorus implant used to form the n type region. Since either the photoresist or the silicon dioxide layer is sufficiently thick to prevent the phosphorus ions from penetrating the silicon, the edge of the photoresist window can be coarsely aligned anywhere on top of the waveguide

#144357 - $15.00 USD Received 23 Mar 2011; revised 22 May 2011; accepted 23 May 2011; published 31 May 2011

and the pn junction will always be formed in the same part of the device. Self-aligned processes are desirable since they allow for a reduction of the fabrication complexity and therefore an increase in device performance repeatability.

Standard process steps are then used to complete the device. Rapid thermal annealing (RTA) is used to electrically activate the implanted impurities. RTA is advantageous over other annealing processes as it results in a high level of electrical activation whilst minimising dopant diffusion. Some degree of diffusion is unavoidable and under the anneal conditions used for this device (1050°C for 10 seconds) n-type dopant diffusion is expected to cause the junction to be positioned within 50nm of the rib edge. To convert between phase and intensity modulation, Mach-Zehnder interferometers (MZI) were used. An asymmetric MZI, where one of the waveguide arms is 180μm longer than the other, is employed to allow accurate analysis of the DC phase modulation. The entire device therefore comprises three sections which must be precisely designed to ensure a high performance; these include the passive optical structure, the phase shifter and the RF coplanar waveguide electrodes.

An optimal passive structure will provide a large extinction ratio with low optical loss over a broad operational wavelength range. The component which splits and then recombines the light between the two MZI arms to a large extent dominates these characteristics. There are a variety of optical structures capable of this function and in this case 2x1 Multi Mode Interferometers (MMIs) are employed. To ensure a large extinction ratio the optical power in the two MZI arms should be precisely balanced which requires the losses in either arms to be equal and precise 50:50 splitting and combining. MMIs are superior in this respect largely due to their insensitivity to slight fabrication defects. Furthermore they are relatively simple to fabricate and can be designed to be compact, have low optical loss and operate over a wide wavelength range. Our previous analysis has estimated losses down to 0.5dB/MMI and demonstrated that they result in passive extinction ratios in excess of 30dB when incorporated into an MZI [16]. To ensure equal optical losses the phase modulator structure was incorporated into both MZI arms. The waveguide structure itself can also affect the overall performance of the device. The width and slab height can be varied to optimise the optical performance of the waveguide in terms of the loss and modal properties. Varying the waveguide dimensions will also affect the performance of the phase shifter so both need to be considered in parallel when selecting appropriate values. Increasing the waveguide width has the effect of reducing the optical loss due to a decreased interaction of the optical mode with sidewall roughness. In terms of the phase shifter, a larger waveguide width tends to increase the modulation efficiency since more of the optical mode is confined within the waveguide and therefore a greater interaction with the varying depletion region occurs. The upper limitation of the waveguide width is the point at which the waveguide supports higher order modes which will significantly degrade the performance of the MZI. This point is also dependent on the slab height. Larger slab heights tend to allow for larger waveguide widths whilst maintaining single mode operation. In terms of the phase shifter a larger slab height reduces access resistance to the pn diode thus increasing the modulation bandwidth. It will however reduce the confinement of the mode within the waveguide resulting in a lower modulation efficiency. Considering the above factors, the modelling process suggests an optimal performance with waveguide dimensions of slab height 100nm and waveguide width 400nm. The waveguide height is fixed by the silicon-on-insulator overlayer thickness which is 220nm.

The performance of the phase shifter is affected firstly by the waveguide dimensions as previously mentioned. With these parameters fixed the positions of the doped regions and the concentration of active dopants within them remain to be optimised. To ensure low access resistance to the diode and therefore a large modulation bandwidth the p+ and n+ regions of target concentration 1e20cm^{-3} should be positioned as close to the waveguide as possible whilst not significantly increasing optical loss due to the interaction with the propagating light. Modelling has indicated that doping-rib edge separations of 450nm and 500nm for the

#144357 - $15.00 USD Received 23 Mar 2011; revised 22 May 2011; accepted 23 May 2011; published 31 May 2011

p+ and n+ regions respectively ensures a modulation bandwidth compatible with 40Gbit/s whilst maintaining low optical loss. Increasing the doping concentrations of the p and n type regions will also increase the modulation bandwidth as well as the modulation efficiency at the expense of increased optical loss. The balance of the doping densities in these two regions will also dictate the modulation efficiency of the device. The work of Soref et al. [17] concluded that modulation by free holes provides a larger change in refractive index with lower optical absorption as compared to modulation by free electrons. For this reason the rib region, which carries the majority of the optical power is doped p type. To obtain a large modulation efficiency, maximal overlap of the optical mode with the region of the device which becomes depleted during the application of a reverse bias is required. In this case the target concentration of active dopants in the n type region ($1.5e18cm^{-3}$) is made much larger than in the p type region ($3e17cm^{-3}$) to ensure that the depletion region extends mainly into the waveguide. With these doping concentrations and positions the theoretical series conductance of the diode excluding contact resistance is approximately 154S/m. Device modelling demonstrates that at 0V the depletion region width (taken at the $1e17\ cm^{-3}$ level) is approximately 60nm, almost entirely extending into the waveguide region. At 6V the depletion region width is approximately 200nm, extending 170nm into the waveguide and 30nm into the slab region. This resulting modal overlap provides a modelled device modulation efficiency of approximately 2.5V.cm between 0V and 6V and 2.2V.cm between 0V and 3V [14]. The modelled phase shifter optical loss (excluding passive waveguide loss) is 1.63dB/mm and 1.33dB/mm at 0V and 6V respectively. An intrinsic modulation bandwidth in excess of 47GHz is predicted.

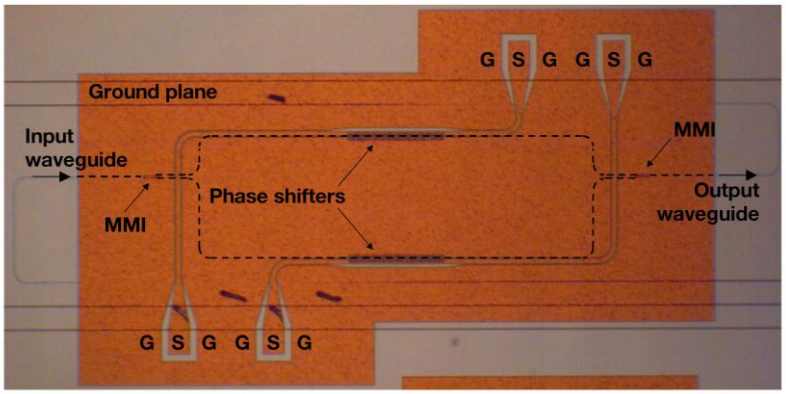

Fig. 3. Microscope image of a fabricated MZI modulator with 250 micrometer long phase modulators. The diagram is annotated to show the position of the waveguides.

The RF coplanar waveguide electrodes should allow the electrical signal to co-propagate along the device at a similar velocity to the light within the waveguide with minimal loss. The electrodes are formed in a stack of the following materials and thicknesses: Ti (30nm), TiN (60nm), AlCu (1300nm), Ti (10nm) and TiN (40nm). This metallisation has been selected to minimise RF loss. The electrodes should also be designed to have an impedance of 50Ohms, including the effects of the phase modulator, in order to reduce reflections of the RF signal and therefore maximise transfer of the RF signal from the source to the device. In order to achieve the correct impedance ADS was first employed to simulate the coplanar waveguide design without the phase modulator. The parameters of characteristic impedance and phase velocity can then be extracted. Using these parameters the impedance and capacitance per unit length may be calculated. The theoretical capacitance of the diode (200pF/m) may then be added to the capacitance of unloaded coplanar waveguide and the overall characteristic impedance estimated. A range of different track width and gap combinations were considered, in this case a track width of 9.1μm was used. The modulators reside in 4μm wide gaps

#144357 - $15.00 USD Received 23 Mar 2011; revised 22 May 2011; accepted 23 May 2011; published 31 May 2011

between the signal track and the ground plane and the resulting electrode to waveguide rib edge separation is therefore 1.8μm. As can be seen in Fig. 3, electrode pads with widened track (44μm) and gap widths (16μm) are positioned at the extremities of the device, perpendicular to the optical input to allow ease of testing. As well as at the input, an electrode pad is used at the end of the line to allow termination with a 50 Ohm load. A microscope image of a fabricated MZI is shown in Fig. 3. The image is annotated to show the positions of the different elements and the waveguides.

3. Experimental results

The devices were tested optically by injecting light from a tunable laser source into the rib waveguides via a surface grating coupler etched into the waveguide. Light was then collected from the other end of the device via a second grating coupler and passed via optical fibre to a detector. The devices have been tested only in single drive where only one arm of the MZI is driven at any one time as this allows isolation of the performance of the phase shifter. It is broadly acknowledged that once the device is integrated into a CMOS chip the transition in operation between single-drive and dual-drive (or push-pull) would be straightforward and would yield reductions in device loss, drive voltage, power consumption and/or device footprint. The phase efficiency of the device is analysed by observing the magnitude of the shift in the spectral response of the asymmetric MZI with applied reverse bias. This can then be converted to phase shift by relating it to the free spectral range of the MZI spectra. The spectral response of the 3.5mm MZI and 1mm MZI are shown in Figs. 4 and 5 respectively for reverse bias voltages between 0V and 8V. The resulting phase shift against voltage is shown in Fig. 6.

The efficiency of the modulator can be expressed as the voltage-length product for a π radian phase shift. In this case, the efficiency is approximately 2.7V.cm. It can be seen in Fig. 4 that this allows for large DC extinction ratios to be achieved from the 3.5mm MZI operated around the quadrature point. For example, using a 4V voltage differential, with the wavelength set at 1536.1nm (corresponding to the quadrature point for a 2V reverse bias) an extinction ratio of approximately 10dB can be obtained. With a 6V differential the extinction ratio increases to 25dB (wavelength 1536nm).

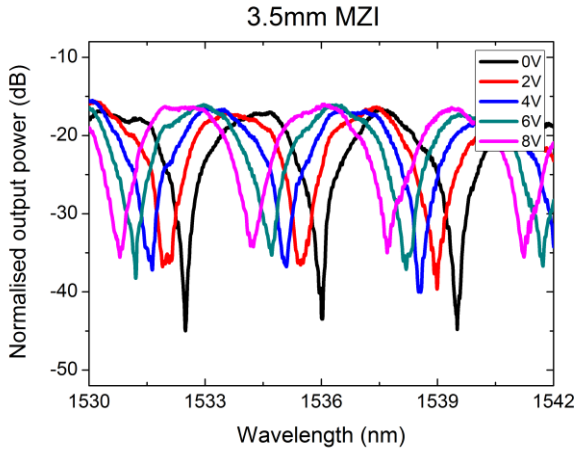

Fig. 4. Graph showing the spectral response of the 3.5mm MZI with different reverse bias voltages

#144357 - $15.00 USD Received 23 Mar 2011; revised 22 May 2011; accepted 23 May 2011; published 31 May 2011

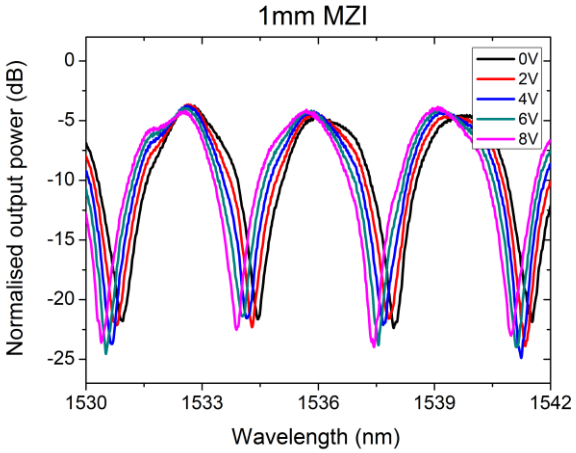

Fig. 5. Graph showing the spectral response of the 1mm MZI with different reverse bias voltages

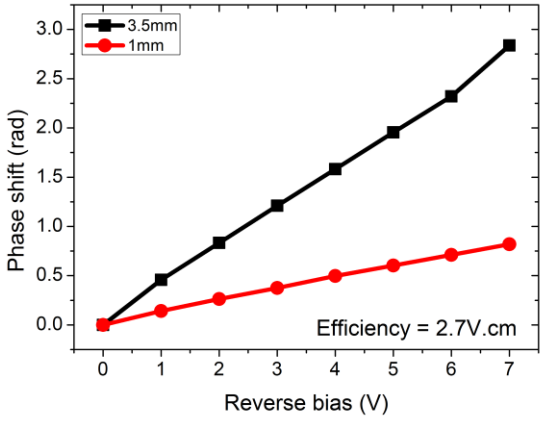

Fig. 6. Phase shift achieved for different reverse bias voltages applied to both 3.5mm and 1mm phase shifters.

The optical loss at the peak of the response for the 1mm and 3.5mm MZI respectively is approximately 5dB and 15dB. From these figures the loss of each MMI and the phase shifter loss can be extracted as 0.5dB and 4dB/mm respectively. The curves of Figs. 4 and 5 are normalised to waveguides of the same length as the MZI and therefore the passive waveguide loss, which from previous analysis is expected to be less than 0.5dB/mm, is normalised out. The optical loss of the phase shifter decreases by approximately 0.4dB/mm when a 6V reverse bias is applied, this indicates the loss caused by the carriers which are producing modulation and causes the variations in extinction ratio at different bias voltages as can be observed in Figs. 4 and 5. The remaining loss, 3.6dB/mm, is approximately three times higher than modelled which suggests that there is scope for further optimisation of the insertion loss. One possible cause for the higher than expected optical loss is lattice damage caused during ion implantation and not fully repaired during annealing. In this case the annealing process can be optimised to minimise the concentration of remaining defects. Another explanation is that the implantation recipes are not optimised. The modelled voltage induced changes in phase and loss, however agree with the experimental values to within 8% and 25%

#144357 - $15.00 USD Received 23 Mar 2011; revised 22 May 2011; accepted 23 May 2011; published 31 May 2011

respectively and therefore this is expected to account for only a small proportion of the additional loss produced. Finally the highly doped p and n type regions could be positioned closer to the waveguide than intended, due to diffusion of the implanted doping towards the waveguide and/or misalignment of the doping window definition. The diode series conductivity estimated from its current-voltage (IV) characteristics is 160S/m and is larger than the theoretical value (which also excluded contact resistance). This suggests that this hypothesis could be valid. To overcome these problems the positions of the highly doped regions can be offset on the mask to account for the diffusion process, in future device iterations. An extension of the self-aligned process can be used to also form the highly doped regions and therefore avoid additional losses caused by errors in their alignment. It should be noted that according to our modelling data [14] a modulation bandwidth compatible with 40Gbit/s is maintained with the doped regions positioned correctly.

The high speed performance of the modulator has been analysed in terms of its ability to convert a stream of electrical data into an optical counterpart. A PRBS unit was used to provide a 40Gbit/s data signal and was fed through an RF amplifier to boost the peak to peak voltage to approximately 4V or 6.5V. The data signal was then passed through a bias tee to allow the voltage level of the data signal to be offset, to ensure the device operates only in depletion mode. The drive signal was launched onto the silicon sample by means of a high speed probe with Ground-Signal-Ground (G-S-G) tip configuration, which connects respectively to the coplanar waveguide pad. The end of the electrode was terminated with a 50Ohm load using another high speed probe and DC block. The wavelength of the optical source was then set to correspond to the quadrature point of the asymmetric MZI spectral response. The optical output was passed through an Erbium Doped Fibre Amplifier (EDFA) and a band pass filter to a digital communications analyser (DCA) with 65GHz optical head. The output optical eye diagrams at 40Gbit/s from both the 1mm and 3.5mm MZIs are shown in Figs. 7-10. An open eye at 40Gbit/s can be observed for both device lengths. The 3.5mm modulator demonstrates modulation depths of 10dB and 7dB when driven with RF peak to peak signals of 6.5V and 4V respectively. The 1mm MZI modulator driven with a 6.5V signal demonstrates a modulation depth of 3.5dB when operated at quadrature and 7.5 dB when operated at −3dB below quadrature (i.e. for an insertion loss of an extra 3dB, the modulation depth can be doubled).

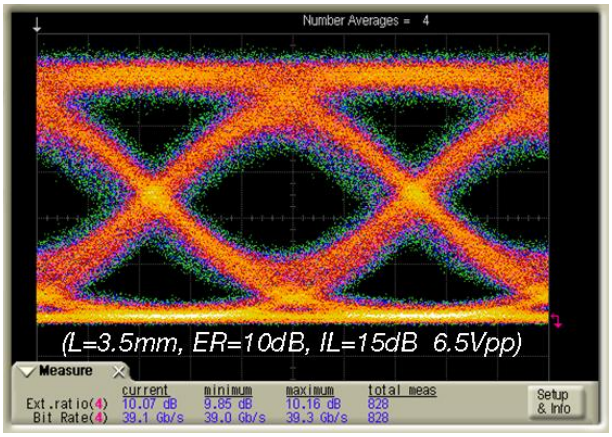

Fig. 7. Eye diagram derived from optical PRBS data output at 40Gbit/s. 3.5mm MZI with 6.5V RF signal operated at quadrature (10dB ER).

#144357 - $15.00 USD Received 23 Mar 2011; revised 22 May 2011; accepted 23 May 2011; published 31 May 2011

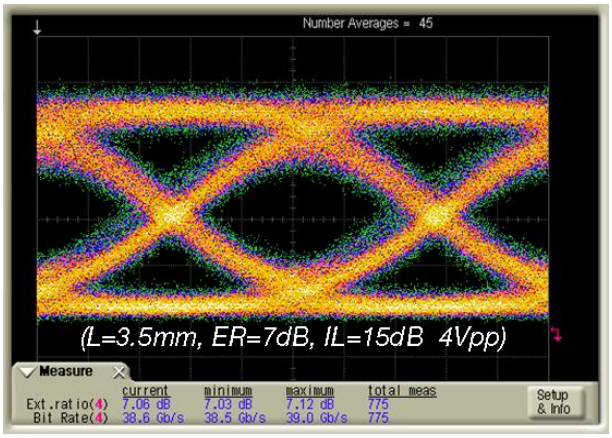

Fig. 8. Eye diagram derived from optical PRBS data output at 40Gbit/s. 3.5mm MZI with 4V RF signal operated at quadrature (7dB ER).

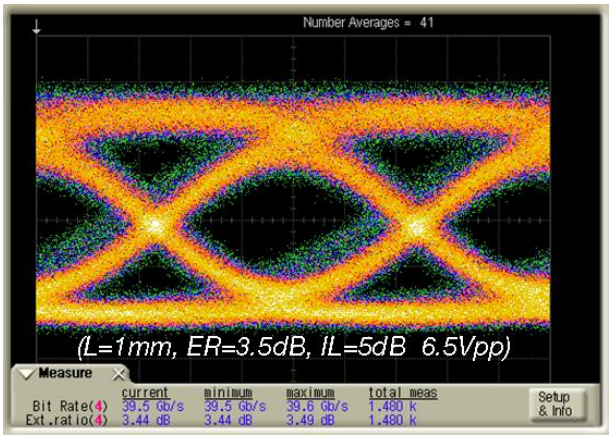

Fig. 9. Eye diagram derived from optical PRBS data output at 40Gbit/s. 1mm MZI with 6.5V RF operated at quadrature (3.5dB ER).

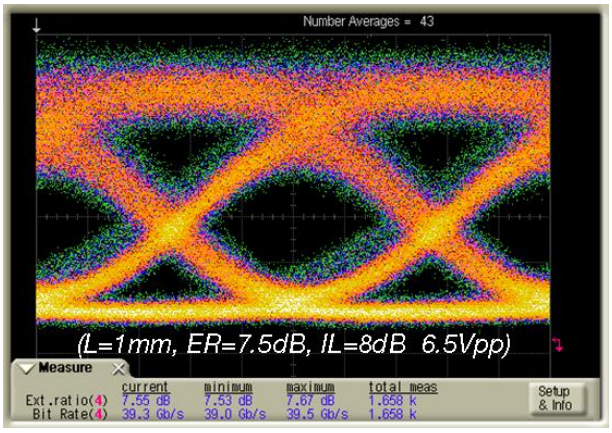

Fig. 10. Eye diagram derived from optical PRBS data output at 40Gbit/s. 1mm MZI with 6.5V RF operated approximately 3dB below quadrature (7.5dB ER).

The power consumption of any device is an important factor to consider. Any RF power delivered by the driver, will either be consumed by the modulator, or will be dissipated in the

#144357 - $15.00 USD Received 23 Mar 2011; revised 22 May 2011; accepted 23 May 2011; published 31 May 2011

50Ohm termination, The DC bias voltage will not reach the termination due to use of a DC block. Therefore the power consumption of the overall device can be calculated by the following expression 1. Where V_{Drive} is the peak to peak voltage of the input drive signal, Z is the impedance of the system and BR the bit rate. Consequently the power consumption can be evaluated to be 2pJ/bit for the 4V drive signal. If a 6.5V drive is used this figure increases to 5.2pJ/bit, but the associated improvement in modulation depth accompanies the increase in power consumption.

$$P = \left(\frac{\left(\frac{1}{2} V_{drive} \right)^2}{Z \times BR} \right) \tag{1}$$

Comparing directly with the current state of the art modulator with a data rate of 40Gbit/s [15] for the same device length (1mm), the total on chip loss is approximately 4dB, whereas for this device it is approximately 5.5dB. The modulation efficiency is 2.7V.cm as opposed to 4V.cm for the device of [15]. The modulation depths are approximately 3.5dB and 1dB respectively at 40Gbit/s. The power consumption using the above calculation for the device of [15] is 16pj/bit compared with 5.3pj/bit for this device (the difference is mainly due to the 14Ohm termination used in [15]). In this case 40Gbit/s modulation has also been achieved over a longer length phase shifter which allows for larger phase shifts to be produced and therefore a larger modulation depth. It can also allow for a lower drive voltage, which will in turn reduce the power consumption of the device. A larger optical loss will however result. With 40Gbit/s modulation achievable from both 1mm and 3.5mm device lengths there is the possibility to select any device length in this range to achieve the required performance metrics in terms of the modulation depth, drive voltage and optical loss, and to therefore tailor the device for specific applications.

4. Conclusion

In this work 40Gbit/s optical modulation in silicon is demonstrated with a large modulation depth for the first time. Phase modulators with an efficiency of 2.7V.cm have been incorporated into Mach-Zehnder Interferometers with 3.5mm and 1mm length arms. Modulation depths of up to 10dB have been demonstrated at 40Gbit/s from the 3.5mm MZI, with a corresponding optical loss of approximately 15dB. Using the 1mm MZI, a lower loss (~5dB) and smaller footprint is demonstrated, although the modulation depth reduces to 3.5dB. If the operating point of the 1mm MZI is moved to 3dB below quadrature, the modulation depth increases to more than 7dB. The combined power consumption of the phase shifter and termination is 2pj/bit or 5.3pj/bit when operated with a 4V and 6.5V peak to peak data signal respectively. This demonstration firstly makes 40Gbit/s optical modulation in silicon viable for commercial applications for the first time, and secondly shows how the device can be modified to suit specific applications simply by varying the active length.

Acknowledgements

The research leading to these results has received funding from the European Community's Seventh Framework Programme (FP7/2007-2013) under grant agreement n 224312 HELIOS and from the EPSRC in the UK to support the UK Silicon Photonics project.

#144357 - $15.00 USD Received 23 Mar 2011; revised 22 May 2011; accepted 23 May 2011; published 31 May 2011